



# DFT Approach on Arsine and Phosphine Gases Adsorption at the Surface of B<sub>16</sub>C<sub>16</sub> Nanocluster

Shaghayegh Ariaei✉

Department of Chemical Engineering, Science and Research Branch, Islamic Azad University, Tehran, Iran

Received: 25 November 2020 / Accepted: 22 December 2020 / Published Online: 30 December 2020

Copyright © 2020 to Lab-in-Silico as a Member of SciEng Publishing Group (SciEng)

**ABSTRACT.** In this study, interactions of arsine (AsH<sub>3</sub>) and phosphine (PH<sub>3</sub>) gas molecules with B<sub>16</sub>C<sub>16</sub> nanocluster were investigated using M06-2X/6-311G(d,p) density functional theory (DFT) method. Results showed that the electron density of adsorbed molecules could play an important role in adsorption of AsH<sub>3</sub> and PH<sub>3</sub> at the surface of B<sub>16</sub>C<sub>16</sub> (on the top of B and C atoms of the cluster). Calculated amounts of adsorption energy were -3.50 and -2.90 eV for AsH<sub>3</sub> and PH<sub>3</sub>, respectively. It revealed that the B<sub>16</sub>C<sub>16</sub> nanocluster could work selectively for adsorbing each of AsH<sub>3</sub> and PH<sub>3</sub> gas molecules. The obtained achievement was approved regarding the calculated properties of molecular orbital energies, band gap, and charge transfer for the optimized systems.

**KEYWORDS.** Arsine; Phosphine; Adsorption; Nanocluster; DFT.

**INTRODUCTION.** Since the innovation of carbon nanotube (CNT) in 1991, considerable attempts have been done for synthesis, characterization, and understanding of such wide surface area nano-scale materials.<sup>1-5</sup> With high surface to volume ratio, nano-scale materials could work as adsorbents for several other substances.<sup>6-10</sup> Generally, nanostructures are defined with their nano-scale dimensions, in which nanoparticles, quantum dots, nanorods, nanowires, thin films, and some types of bulk materials could be categorized in these materials list.<sup>11</sup> Carbon based nanostructures such as graphene, fullerene, and CNT, have always attracted the attention of researchers due to their remarkable properties.<sup>12-15</sup> Fullerene and fullerene-like clusters have been seen as fantastic materials for adsorption functions.<sup>16</sup> Such materials could be used in many areas and they are particularly significant in pollutants removal of environmental applications.<sup>17</sup> In the current industrial and modern world, air and water pollutions are serious issues almost all around the world. Therefore, thinking about

how to remove the pollutants from the living environment is an important task to maintain the human health quality. In this regard, considerable research activities have been directed toward the development of new adsorbents particularly using nanostructures for such pollutant diagnosis and removals.<sup>18-20</sup> Based on physicochemical properties, fullerenes have been seen as promising adsorbents for various organic pollutants and metal ions.<sup>21</sup> Moreover, fullerenes could be easily modified by chemical treatment in order to improve their adsorption capacity and function.<sup>22</sup>

During the last decade, many research works have been carried out to fabricate various fullerene-like materials in order to characterize their features for specific applications.<sup>23-25</sup> Previously, boron carbide (BC) fullerene-like materials have been introduced for their characteristic features of high temperature stability, low dielectric constant, large thermal conductivity, and oxidation resistance, favorable for various electronic related applications.<sup>26</sup>

✉ Corresponding author; E-mail address: shaghayeghariaei9595@gmail.com (S. Ariaei).

Arsine (AH<sub>3</sub>) and phosphine (PH<sub>3</sub>) are toxic gas molecules in the air in addition to potential flammability; therefore, their detection and removal from environment is a crucial task.<sup>27</sup> In this work, a model of B<sub>16</sub>C<sub>16</sub> nanocluster was investigated for adsorbing each of AH<sub>3</sub> and PH<sub>3</sub> gas molecules. To achieve the purpose, density functional theory (DFT) calculations were performed to obtain optimized structures and properties to examine the adsorbent role of B<sub>16</sub>C<sub>16</sub> nanocluster for AH<sub>3</sub> and PH<sub>3</sub> gas molecules.

**METHODOLOGY.** Within this work, a representative model of B<sub>16</sub>C<sub>16</sub> fullerene-like nanocluster was investigated to recognize its features for adsorbent of AH<sub>3</sub> and PH<sub>3</sub> gas molecules (Figs. 1 and 2). DFT calculations were performed using the M06-2x method and the 6-311G(d,p) basis set as implemented in the GAMESS program.<sup>28</sup> All the structures were optimized to achieve the minimized energy geometries, in which they were confirmed through

vibrational frequency calculations avoiding imaginary frequencies. Natural bonding orbital (NBO),<sup>29</sup> density of states (DOS),<sup>30</sup> molecular electrostatic potential (MEP),<sup>31</sup> were all analyzed for the optimized systems. A very important parameter in the gas adsorption process is the cohesion amount of gaseous chemical species at the surface of adsorbent, which could be evaluated as adsorption energy ( $E_{\text{ads}}$ ) using eq. (1).

$$E_{\text{ads}} = E_{(\text{adsorbate@cluster})} - E_{(\text{adsorbate})} - E_{(\text{cluster})} \quad (1)$$

$E_{(\text{adsorbate@cluster})}$  is the total energy of complex of each absorbed AH<sub>3</sub> and PH<sub>3</sub> molecules at the surface of B<sub>16</sub>C<sub>16</sub> nanocluster,  $E_{(\text{cluster})}$  and  $E_{(\text{adsorbate})}$  are the total energies of the pristine nanocluster and each of singular gas molecules. All the results of this work were summarized in Table 1 and Figs. 1-4. It is worth to note that such detailed information about complicated structures systems could be very well recognized based on computer-based works prior to or in complementary experiments.<sup>32-46</sup>

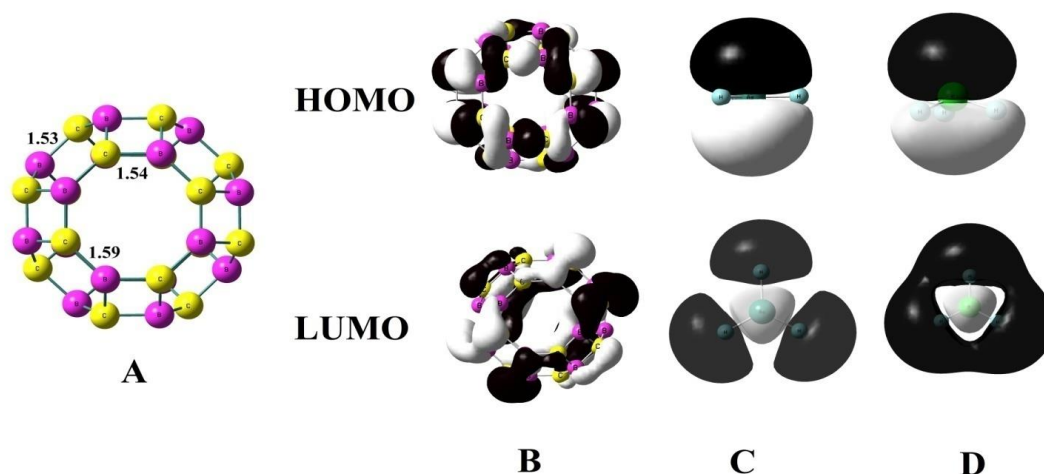


**Fig. 1:** A) B<sub>16</sub>C<sub>16</sub> nanocluster, B) HOMO and LUMO patterns of B<sub>16</sub>C<sub>16</sub>, C) HOMO and LUMO patterns of AsH<sub>3</sub>, D) HOMO and LUMO patterns of PH<sub>3</sub>.

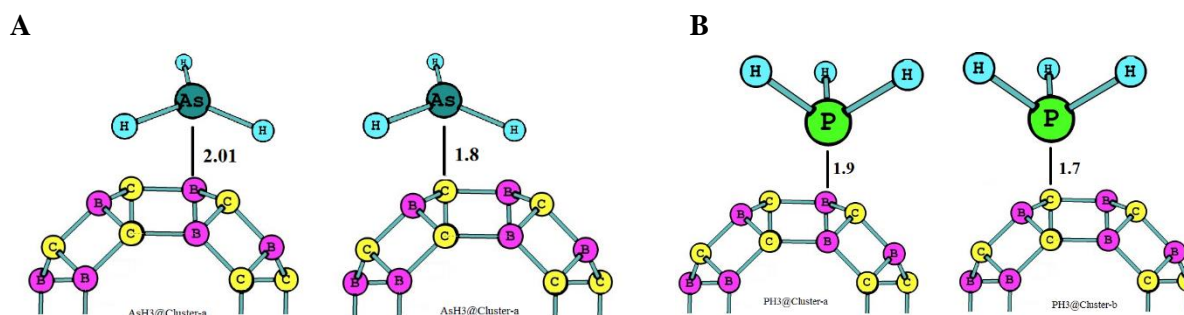


**Fig. 2:** Optimized models of AsH<sub>3</sub>@B<sub>16</sub>C<sub>16</sub> (A) and PH<sub>3</sub>@B<sub>16</sub>C<sub>16</sub> (B). Interacting distances are in Å.

**RESULTS & DISCUSSION.** Fig. 1 demonstrates the structure of optimized pristine B<sub>16</sub>C<sub>16</sub> nanocluster consisting of eight four-membered (4MR), eight six-membered (6MR) and two eight-membered (8MR) rings with bond lengths of 1.54, 1.53, and 1.59 Å. The value of 4.09 eV was evaluated for energy gap ( $E_g$ ) of the B<sub>16</sub>C<sub>16</sub> nanocluster, showing the energy difference between the highest occupied and the lowest unoccupied molecular orbital (HOMO and LUMO) levels. As shown in Fig. 1B, the HOMO and LUMO patterns of B<sub>16</sub>C<sub>16</sub> were distributed at the C and B atomic sites, respectively. In order to find the

optimized adsorption configuration for each of AsH<sub>3</sub> and PH<sub>3</sub> gases at the nanocluster surface (AsH<sub>3</sub>@nanocluster and PH<sub>3</sub>@nanocluster) (Fig. 2), the molecules were initially placed at different positions above the B<sub>16</sub>C<sub>16</sub> nanocluster with different orientations. After full geometrical relaxation during optimization processes, stabilized configurations were extracted for the purpose of this work (Fig. 2). The calculated values of  $E_{ads}$  varied from -2.92 to -3.50 eV for AsH<sub>3</sub>@nanocluster and from -1.61 to -2.90 eV for PH<sub>3</sub>@nanocluster interacting complexes as summarized in Table 1.

**Table 1:** Evaluated properties for the models.\*

Configuration	$E_{ads}$ eV	$E_{br}$ eV	Homo eV	LUMO eV	$E_g$ eV	$\Delta E_g$ eV	QT
B <sub>16</sub> C <sub>16</sub>	N/A	N/A	-7.62	-3.53	4.09	N/A	N/A
AsH <sub>3</sub> @ B <sub>16</sub> C <sub>16</sub> -a	-2.92	0.25	-6.82	-3.21	3.61	0.48	0.72
AsH <sub>3</sub> @ B <sub>16</sub> C <sub>16</sub> -b	-3.50	1.09	-6.95	-3.23	3.72	0.37	1.04
PH <sub>3</sub> @ B <sub>16</sub> C <sub>16</sub> -a	-1.61	0.14	-6.84	-3.21	3.63	0.46	0.71
PH <sub>3</sub> @ B <sub>16</sub> C <sub>16</sub> -b	-2.90	0.17	-6.92	-3.26	3.66	0.43	1.00

\*  $E_{ads}$  implies for adsorption energy,  $E_{br}$  implies for bond reorganization energies,  $E_g$  implies for energy gap indicated by energy difference of HOMO and LUMO levels,  $\Delta E_g$  implies for energy difference of  $E_g$  between pure and gas-adsorbed nanoclusters, QT implies for net partial charge on small gas molecule.

AsH<sub>3</sub> and PH<sub>3</sub> molecules were selected as target adsorbates. Full structural optimizations were carried out on the B<sub>16</sub>C<sub>16</sub> nanocluster with and without each of AsH<sub>3</sub> and PH<sub>3</sub> molecules to achieve electronic properties in addition to the minimized energy geometries. For each molecule, a number of orientations as well as different adsorption sites on the nanocluster surface were probed in order to find the lowest energy configuration for the adsorbate@adsorbent complex systems. After full relaxation, stabilized configurations were obtained (Fig. 2). More detailed information including values of  $E_{ads}$ , equilibrium adsorbate...adsorbent distance, bond reorganization energy ( $E_{br}$ ), change of  $E_g$  of nanocluster upon the adsorption process ( $\Delta E_g$ ) and NBO charge transfer (QT) were listed in Table 1. All the information were provided to explore the adsorption process for each of AsH<sub>3</sub> and PH<sub>3</sub> gas molecules, one by one.

AsH<sub>3</sub>@B<sub>16</sub>C<sub>16</sub>. Several configurations were considered in order to study the adsorption of AsH<sub>3</sub> at the nanocluster surface. AsH<sub>3</sub> molecule was placed above the B and C atom, in which AsH<sub>3</sub> molecule was oriented perpendicular to the nanocluster. After full relaxation, two configurations were found to be stable, in which

the axis of adsorbed AsH<sub>3</sub> was aligned diagonal to the nanocluster surface; AsH<sub>3</sub> from As head was adsorbed on the top of B and C atoms of the nanocluster (Fig. 2). The calculations showed that the adsorptions of AsH<sub>3</sub> molecule from its As head on the top of B and C atoms were exothermic processes with negative  $E_{ads}$  of -2.92 and -3.50 eV and the interaction distance of 2.01 and 1.8 Å (Fig. 2). This interaction led to a charge transfer of 0.72 and 1.04 |e| from the AsH<sub>3</sub> to the nanocluster (Table 1), indicating that AsH<sub>3</sub> acted as an electron donor and the cluster acted as an electron acceptor. The calculated MEP (Fig. 3) obviously showed this phenomenon where the blue color on the adsorbed AsH<sub>3</sub> represented the positive charge. The interaction between AsH<sub>3</sub> and nanocluster became stronger. To explain this result, FMO analyses were performed on AsH<sub>3</sub> molecule. It showed that HOMO was slightly more localized on the As atom (Fig. 1); therefore, the interaction between the As head of AsH<sub>3</sub> and B atom (LUMO) of nanocluster was suitable. However, LUMO localization on the C atom was stronger, indicating that the AsH<sub>3</sub> formed chemical bonding with the nanocluster. Thus, the B<sub>16</sub>C<sub>16</sub> nanocluster worked selectively against adsorbing AsH<sub>3</sub>.

PH<sub>3</sub>@B<sub>16</sub>C<sub>16</sub>. PH<sub>3</sub> molecule was initially placed towards various sites of nanocluster with different orientation to find the optimal adsorption. The favorable configuration of PH<sub>3</sub> at the nanocluster surface was shown in Fig. 2. The interaction between P atom of PH<sub>3</sub> molecule and B and C atom of the nanocluster revealed that after full relaxation, two stable configurations were obtained. The axis of adsorbed PH<sub>3</sub> was aligned perpendicular to the nanocluster surface. This process was exothermic with E<sub>ads</sub> of -1.61 and -2.90 eV and the molecule-nanocluster distance was about 1.9 and 1.7 Å. The interaction between PH<sub>3</sub> and the cluster led to charge transfer of 0.71 and 1.00 |e| from the PH<sub>3</sub> to the nanocluster (Table 1). To explain this result, FMO analyses were performed on PH<sub>3</sub> molecule and the results showed that its HOMO was more localized on the P atom (Fig. 1.); therefore, the interaction between the P head of PH<sub>3</sub> and LUMO of nanocluster localized on C atom was stronger. This finding indicated that the PH<sub>3</sub> connected to the nanocluster with strong chemical bonding. Thus, the B<sub>16</sub>C<sub>16</sub> nanocluster could work selectively as an adsorbent of PH<sub>3</sub>.

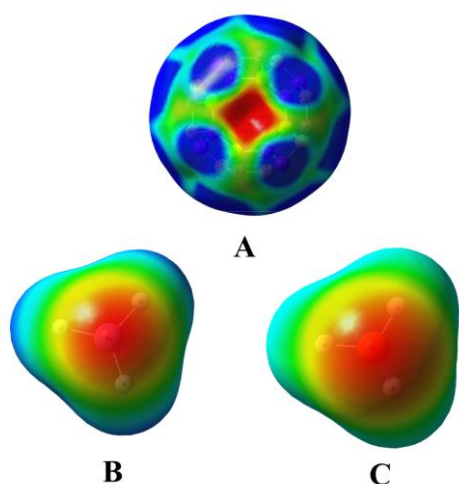


**Fig. 3:** Molecular electrostatic potential (MEP) surfaces for B<sub>16</sub>C<sub>16</sub> nanocluster (A), AsH<sub>3</sub> (B), and PH<sub>3</sub> (C). The surfaces are defined by the 0.0004 electrons/b<sup>3</sup> contour of the electronic density. Color ranges, in a.u., are: blue, more positive than 0.050; red, more negative than -0.050.

MEP Analyses. The charge distribution could be explained by MEP calculations. AsH<sub>3</sub> and PH<sub>3</sub> cases were selected and MEP surfaces were computed for the B<sub>16</sub>C<sub>16</sub> nanocluster and AsH<sub>3</sub> and PH<sub>3</sub> adsorbed complexes. MEP is the potential generated by the charge distribution of the molecule, in which the atomic site could be defined using eq. (2).

$$V(r) = \sum_A \frac{Z_A}{|R_A - r|} - \int \frac{\rho(r') dr'}{|r' - r|} \quad (2)$$

Z<sub>A</sub> is the charge on nucleus A, located at R<sub>A</sub>. The sign of V(r) depends on whether the effects of the nuclei or the electrons are dominant at any point. The MEP has frequently been used to explore the chemical properties of several materials. As shown in Fig. 3, B atom were positively charged (blue colors) whereas C atoms were negatively charged (red colors) in B–C bonds of nanocluster surface. It indicated that a large charge was transferred from B atoms to C ones resulted in a strong ionic bonding in B–C nanocluster surface.

DOS Analyses. To verify effects of the adsorption of AsH<sub>3</sub> and PH<sub>3</sub> molecules on electronic properties of the nanocluster, total electronic densities of states (DOS) of adsorbate@nanocluster complexes were calculated and the results were shown in Fig. 4. These plots revealed that for all complexes the DOS was near the Fermi level and was affected by the molecule adsorption in all related complexes. Values of ΔE<sub>g</sub> (change of the value of E<sub>g</sub> upon the adsorption process) related to each adsorbate@B<sub>16</sub>C<sub>16</sub> complex system was shown in Table 1. The values of E<sub>g</sub> for the most favorable adsorption configurations of AsH<sub>3</sub> (a,b) and PH<sub>3</sub> (a,b) were 3.61, 3.72, 3.63 and 3.66 eV, respectively. Consistent with the values of E<sub>ads</sub>, the DOS analysis also indicated that the interaction between all molecules and the nanocluster were stable. However, for all adsorbate@nanocluster complexes, the interaction caused a change in the DOS on both sides of the Fermi level in comparison with that of the pristine nanocluster. As a result, for both gases, the system became more semiconductor-like. This proceeding led to a fundamental change in the electrical conductivity of cluster regarding eq. (3).

$$\sigma \propto \exp\left(\frac{-E_g}{2kT}\right) \quad (3)$$

σ implies for electrical conductivity and k implies for the Boltzmann's constant. The concept of Eq. (3) reveals that the smaller the E<sub>g</sub> at specified temperature, the higher electrical conductivity. However, the E<sub>g</sub> of AsH<sub>3</sub>@nanocluster complex was decreased compared to E<sub>g</sub> of pristine nanocluster. According to the dependency between conductivity

and negative value of  $E_g$ , it was predictable that it could become larger with decrease of  $E_g$ . It demonstrated the high sensitivity of the electronic properties of  $B_{16}C_{16}$  towards the adsorption of the all molecules. Based on

such obtained results, it was believed that the  $B_{16}C_{16}$  nanocluster could be transformed in the presence of  $AsH_3$  molecule directly into an electrical signal to be detected for  $AsH_3$  adsorption.

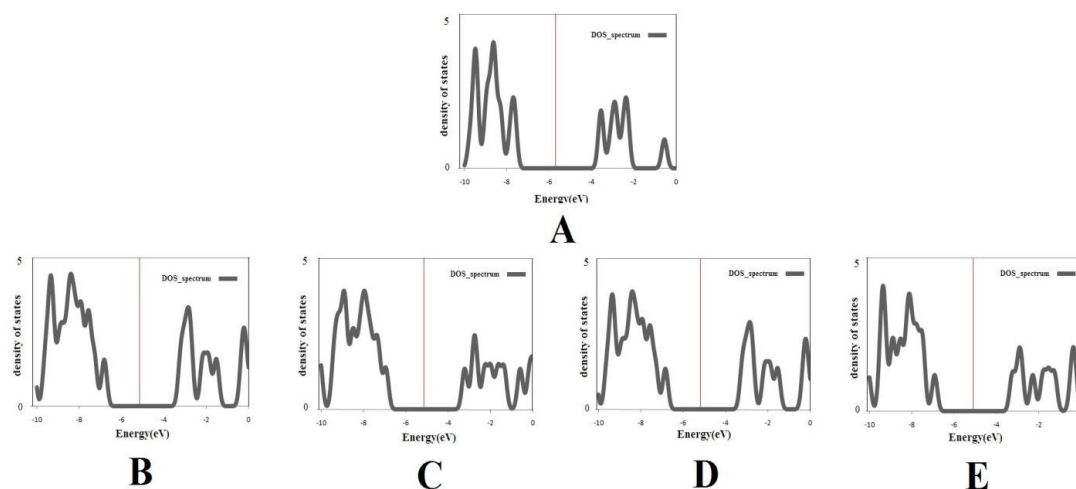


**Fig. 4:** Density of states (DOS) for pristine  $B_{16}C_{16}$  nanocluster (A),  $AsH_3$ @nanocluster-a (B),  $AsH_3$ @nanocluster-b (C),  $PH_3$ @nanocluster-a (D),  $PH_3$ @nanocluster-b (E).

**CONCLUSION.** DFT calculations were performed to study the optimized geometries, stabilities, and electronic properties of  $AsH_3$  and  $PH_3$  molecules adsorbed at the exterior surface of  $B_{16}C_{16}$  nanocluster. It was found that  $AsH_3$  and  $PH_3$  molecules could be

adsorbed at the surface of  $B_{16}C_{16}$  with strong chemical bonding. The  $B_{16}C_{16}$  nanocluster could work selectively as an adsorbent against  $AsH_3$  and  $PH_3$  gas molecules. It was predicted that the  $B_{16}C_{16}$  nanocluster could be useful in for gas detection and removal purposes.

## REFERENCES

- Iijima S. Synthetic nano-scale fibrous matrix. *Nature*. 1991;56:354-358.
- Faramarzi R, Falahati M, Mirzaei M. Interactions of fluorouracil by CNT and BNNT: DFT analyses. *Adv J Sci Eng*. 2020;1:62-66.
- Mirzaei M, Hadipour NL, Seif A, Giahi M. Density functional study of zigzag BN nanotubes with equivalent ends. *Physica E*. 2008;40:3060-3063.
- Nouri A, Mirzaei M. DFT calculations of B-11 and N-15 NMR parameters in BN nanocone. *J Mol Struct THEOCHEM*. 2009;913:207-209.
- Mirzaei M, Hadipour NL. Density functional calculations of 14N and 11B NQR parameters in the H-capped (6, 0) and (4, 4) single-walled BN nanotubes. *Physica E*. 2008;40:800-804.
- Mirzaei M, Mirzaei M. A computational study of oxygen-termination of a (6, 0) boron nitride nanotube. *Monatsh Chem*. 2010;141:491-494.
- Mirzaei M, Mirzaei M. Electronic structure of sulfur terminated zigzag boron nitride nanotube: A computational study. *Solid State Sci*. 2010;12:1337-1340.
- Mirzaei M, Meskinfam M. Computational studies of effects of tubular lengths on the NMR properties of pristine and carbon decorated boron phosphide nanotubes. *Solid State Sci*. 2011;13:1926-1930.
- Mirzaei M, Mirzaei M. The B-doped SiC nanotubes: A computational study. *J Mol Struct THEOCHEM*. 2010;953:134-138.
- Mirzaei M, Mirzaei M. The C-doped AlP nanotubes: A computational study. *Solid State Sci*. 2011;13:244-250.
- Mirzaei M. The NMR parameters of the SiC-doped BN nanotubes: a DFT study. *Physica E*. 2010;42:1954-1957.
- Mirzaei M. Effects of carbon nanotubes on properties of the fluorouracil anticancer drug: DFT studies of a CNT-fluorouracil compound. *Int J Nano Dimens*. 2013;3:175-179.
- Mirzaei M, Yousefi M. Computational studies of the purine-functionalized graphene sheets. *Superlatt Microstruct*. 2012;52:612-617.
- Mirzaei M, Kalhor HR, Hadipour NL. Covalent hybridization of CNT by thymine and uracil: A computational study. *J Mol Model*. 2011;17:695-699.
- Harismah K, Ozkendir OM, Mirzaei M. Lithium adsorption at the  $C_{20}$  fullerene-like cage: DFT approach. *Adv J Sci Eng*. 2020;1:74-79.
- Mirzaei M. Nanotechnology for science and engineering. *Adv J Sci Eng*. 2020;1:67-68.
- Tahmasebi E, Shakerzadeh E. Potential application of  $B_{40}$  fullerene as an innovative anode material for Ca-ion batteries: In silico investigation. *Lab-in-Silico*. 2020;1:16-20.

18. Gupta VK, Saleh TA. Sorption of pollutants by porous carbon, carbon nanotubes and fullerene-An overview. *Environ Sci Pollut Res*. 2013;20:2828-2843.
19. Rikame SS, Mungray AA, Mungray AK. Synthesis, characterization and application of phosphorylated fullerene/sulfonated polyvinyl alcohol (PFSP) composite cation exchange membrane for copper removal. *Separat Purif Technol*. 2017;177:29-39.
20. Khan AA, Ahmad I, Ahmad R. Influence of electric field on CO<sub>2</sub> removal by P-doped C<sub>60</sub>-fullerene: A DFT study. *Chem Phys Lett*. 2020;742:137155.
21. Ong SL, Hu JY, Biryulin YF, Polotskaya GA. Fullerene-containing polymer membranes for rejection of estrogenic compounds in water. *Full Nano Carbon Nonstruct*. 2006;14:463-466.
22. Jun LY, Mubarak NM, Yee MJ, Yon LS, Bing CH, Khalid M, Abdullah EC. An overview of functionalised carbon nanomaterial for organic pollutant removal. *J Indust Eng Chem*. 2018;67:175-186.
23. Baniasadi R, Harismah K, Sadeghi M, Mirzaei M. Adsorption of vitamin C on a fullerene surface: DFT studies. *J Nanoanalys*. 2017;4:1-7.
24. Kouchaki A, Gülseren O, Hadipour N, Mirzaei M. Relaxations of fluorouracil tautomers by decorations of fullerene-like SiCs: DFT studies. *Phys Lett A*. 2016;380:2160-2166.
25. Harismah K, Mirzaei M, Ghasemi N, Nejati M. Non-covalent functionalisation of C<sub>30</sub> fullerene by pyrrole-*n*-carboxylic acid (*n*= 2, 3): Density functional theory studies. *Z Naturforsch A*. 2017;73:51-56.
26. Vergara Reyes HN, Chigo Anota E, Castro M. C<sub>60</sub>-like boron carbide and carbon nitride fullerenes: stability and electronic properties obtained by DFT methods. *Full Nano Carbon Nanostruct*. 2018;26:52-60.
27. Mahabal MS, Deshpande MD, Hussain T, Ahuja R. Sensing characteristics of phosphorene monolayers toward PH<sub>3</sub> and AsH<sub>3</sub> gases upon the introduction of vacancy defects. *J Phys Chem C*. 2016;120:20428-20436.
28. Alexeev Y, P Mazanetz M, Ichihara O, G Fedorov D. GAMESS as a free quantum-mechanical platform for drug research. *Curr Topics Med Chem*. 2012;12:2013-2033.
29. Peralta-Inga Z, Lane P, Murray JS, Boyd S, Grice ME, O'Connor CJ, Politzer P. Characterization of surface electrostatic potentials of some (5, 5) and (n, 1) carbon and boron/nitrogen model nanotubes. *Nano Lett*. 2003;3:21-28.
30. Fallahpour F, Nouraliei M, Gorgani SS. Theoretical evaluation of a double-functional heterogeneous nano-sensor. *Appl Surf Sci*. 2016;366:545-551.
31. Politzer P, Lane P, Murray JS, Concha MC. Comparative analysis of surface electrostatic potentials of carbon, boron/nitrogen and carbon/boron/nitrogen model nanotubes. *J Mol Model*. 2005;11:1-7.
32. Ghamsari PA, Nouraliei M, Gorgani SS. DFT simulation towards evaluation the molecular structure and properties of the heterogeneous C<sub>16</sub>Mg<sub>8</sub>O<sub>8</sub> nano-cage as selective nano-sensor for H<sub>2</sub> and N<sub>2</sub> gases. *J Mol Graph Model*. 2016;70:163-169.
33. Saedi L, Javanshir Z, Khanahmadzadeh S, Maskanati M, Nouraliei M. Determination of H<sub>2</sub>S, COS, CS<sub>2</sub> and SO<sub>2</sub> by an aluminium nitride nanocluster: DFT studies. *Mol Phys*. 2020;118:e1658909.
34. Rostami Z, Maskanati M, Khanahmadzadeh S, Dodangi M, Nouraliei M. Interaction of nitrotyrosine with aluminum nitride nanostructures: A density functional approach. *Physica E*. 2020;116:113735.
35. Mirzaei M, Hadipour NL, Abolhassani MR. Influence of C-doping on the B-11 and N-14 quadrupole coupling constants in boron-nitride nanotubes: A DFT study. *Z Naturforsch A*. 2007;62:56-60.
36. Mirzaei M. Calculation of chemical shielding in C-doped zigzag BN nanotubes. *Monatsh Chem*. 2009;140:1275-1278.
37. Mirzaei M. A computational NMR study of boron phosphide nanotubes. *Z Naturforsch A*. 2010;65:844-848.
38. Gunaydin S, Alcan V, Mirzaei M, Ozkendir OM. Electronic structure study of Fe substituted RuO<sub>2</sub> semiconductor. *Lab-in-Silico*. 2020;1:7-10.
39. Samadi Z, Mirzaei M, Hadipour NL, Khorami SA. Density functional calculations of oxygen, nitrogen and hydrogen electric field gradient and chemical shielding tensors to study hydrogen bonding properties of peptide group (OC-NH) in crystalline acetamide. *J Mol Graph Model*. 2008;26:977-981.
40. Mirzaei M, Hadipour NL, Ahmadi K. Investigation of C-H...OC and N-H...OC hydrogen-bonding interactions in crystalline thymine by DFT calculations of O-17, N-14 and H-2 NQR parameters. *Biophys Chem*. 2007;125:411-415.
41. Mirzaei M, Gülseren O, Hadipour N. DFT explorations of quadrupole coupling constants for planar 5-fluorouracil pairs. *Comput Theor Chem*. 2016;1090:67-73.
42. Yaghoobi R, Mirzaei M. Computational analyses of cytidine and aza-cytidine molecular structures. *Lab-in-Silico*. 2020;1:21-25.
43. Partovi T, Mirzaei M, Hadipour NL. The C-H...O Hydrogen bonding effects on the <sup>17</sup>O electric field gradient and chemical shielding tensors in crystalline 1-methyluracil: A DFT study. *Z Naturforsch A*. 2006;61:383-388.
44. Ozkendir OM. Temperature dependent XAFS study of CrFe<sub>2</sub>O<sub>4</sub>. *Lab-in-Silico*. 2020;1:33-37.
45. Agil H, Akduran N. Structural, electrical and magnetic properties of FeO added GdBaCuO superconductors. *Adv J Sci Eng*. 2020;1:122-127.
46. Mirzaei M. Science and engineering in silico. *Adv J Sci Eng*. 2020;1:1-2.

**How to Cite:** Ariaei S. DFT Approach on Arsine and Phosphine Gases Adsorption at the Surface of B<sub>16</sub>C<sub>16</sub> Nanocluster. *Lab-in-Silico*. 2020;1(2):44-49.

**DOI:** <https://doi.org/10.22034/labinsilico20012044>

**URL:** <https://sciengpub.com/lab-in-silico/article/view/labinsilico20012044>



This work is licensed under a [Creative Commons Attribution 4.0 International License \(CC-BY 4.0\)](https://creativecommons.org/licenses/by/4.0/).